Int. J. Nanosci. Nanotechnol., Vol. 15, No. 1, March. 2019, pp. 55-64

Short Communication

Improving the Thermal Characteristics of Semiconductor Lasers Using a New Asymmetric Waveguide Structure

Zahra Danesh Kaftroudi[1,*] and Abolfazl Mazandarani[2]

[1]Department of Engineering Sciences, Faculty of Technology and Engineering East of Guilan, University of Guilan, 44891- 63157, Rudsar-Vajargah, Iran.
[2]Plasma & Nuclear Fusion Research School, Nuclear Science& Technology Research Institute, Tehran, Iran.

(*) Corresponding author: Zahraadaneh@guilan.ac.ir
(Received: 09 March 2018 and Accepted: 22 May 2018)

Abstract

Self-heating leads to a temperature rise of the laser diode and limits the output power and efficiency due to increased loss and decreased differential gain. To control device self-heating, it is required to design the laser structure with a low optical loss, while the heat flux must spread out of the device efficiently. In this study, a new asymmetric waveguide design is proposed and the thermal performance of the laser with this new design is theoretically analyzed and compared with conventional symmetric waveguide laser. For this purpose, the simulation PICS3D software is used, which self-consistently combines 3D simulation of carrier transport, self-heating, and optical wave-guiding. According to the numerical simulation results, when the asymmetric waveguide is used the semiconductor laser shows a higher output light power and slope efficiency. The results show that Joule heating decreases and recombination heat increases, but heat dissipation occurs more effectively due to increased cooling densities. Overall, the maximum laser operation temperature decreases, confirming that our new asymmetric waveguide structure improves laser thermal characteristics.

Keywords: *Semiconductor laser, Simulation, Asymmetric waveguide, Self-heating.*

1. INTRODUCTION

The performance of the semiconductor laser has been dramatically improved since its invention in 1962. Today, this type of laser is an indispensable part of our life as optical components connecting home and the Internet and long-distance large-capacity trunk networks. Wavelengths used for optical communication are mainly 1.55 μm for long-distance transmission and 1.3 μm for short- and mid-distance transmissions due to the minimum loss and minimum dispersion in optical fiber [1, 2]. InGaAsP-InP material system is widely used in semiconductor laser for optical telecommunication applications because of device reliability and handling in its process. The practical applications of InGaAsP-InP-based lasers have been obstructed by its poor characteristics. One of the major problems in this regard is the thermal property, which is related to the low potential barrier height in the conduction band. For example, the threshold current increases steeply with temperature, and the maximum operating temperature becomes limited [3, 4].

Self-heating leads to a temperature rise of laser diode and limits the output power, efficiency and modulation bandwidth due to the increased loss and decreased differential gain [5, 6]. The main heat sources in laser diode during continuous wave (CW) operation are Joule heating and non-radiative recombination heating. As

current is injected into the laser diode, Joule heating occurs due to semiconductor material intrinsic resistance and the resistance at the heterojunction interfaces. The discontinuity of band structure at heterojunction interface contributes a larger portion of the series resistance. Holes have a lower mobility than electrons so that p-type material has a higher electrical resistance than n-type layers. At the same time, free carrier absorption occurs and generates hot carriers during CW operation [7]. The hot carriers interact with the lattice through phonon emission. When the hot carriers relax to lower energy state, optical phonons are emitted. Lattice temperature is increased when the optical phonons relax into acoustic phonons.

Many physical mechanisms in laser diode are affected at elevated active region temperature. First of all, a bandgap reduction occur leading to the red shift of the gain peak. Fermi level also shifts and becomes closer to the barrier energy level causing wider Fermi distribution of carriers [8]. As a consequence, carriers can be thermally ejected out of the QW into the separate confined layers and peak gain is decreased substantially. Leakage of electrons occurs and decreases the injection efficiency [9]. To maintain the threshold gain, pump power is increased. However, the differential gain is decreased due to broaden Fermi distribution of carriers.

When the carrier density is increased in the QW at higher pump level, stronger Auger recombination and stronger spontaneous recombination occur since these processes depend on the carrier density. Efficiency is further reduced by stronger spontaneous recombination. Stronger Auger recombination adds up more heat to the active region. Free carrier absorption also increases at higher carrier density and increases the internal optical loss. The declined injection efficiency and increased free carrier absorption loss will limit laser diode slope efficiency. Finally, output power is limited by thermal rollover. It needs to be point out that the threshold current will also be increased at elevated temperature due to higher loss and lower injection efficiency [10].

To reduce device self-heating, the design of laser structure must reduce optical loss. The internal optical loss consists of cladding, waveguide, and active region loss. Since long cavity is essential in the semiconductor laser structure to increase the gain for high power operation. The waveguide must be designed with allow loss, which enables a significant increase in cavity length without sacrificing the efficiency. One way to reduce the internal loss by engineering the waveguide design is to use asymmetric waveguide design. Shifting the optical mode to n-cladding can decrease the cladding loss since electrons have smaller free carrier absorption cross section than holes. Meanwhile, active region loss can be reduced since the optical mode overlaps less with the gain region [11]. A significant increase in the brightness has been predicted in tapered lasers with InGaAs–InGaAsP active region asymmetrically located in the optical cavity with a reduced penalty in terms of the threshold current [12]. An asymmetric waveguide nitride laser diode layer structure that uses the p-cladding layer to confine injected electrons was designed. The structure represented a departure from conventional symmetric nitride laser diode structures with a high optical confinement factor [13].

Here, we theoretically propose and analyze a new asymmetric waveguide InGaAsP/InP laser diode construction in order to achieve an optimal thermal performance. We used simulation software PICS3D, which self-consistently combines 3D simulation of carrier transport, self-heating, and optical wave-guiding [14]. Through simulation, the thermal performances of laser diodes with the symmetric and asymmetric waveguides are studied. For the sake of simplicity, they will be called Ref. structure and New

structure, respectively. The simulation results indicate that after using asymmetric waveguide structure, semiconductor laser shows a higher output light power and slope efficiency. Joule heating decreases and recombination heat increases, but heat dissipation occurs more effectively due to increased cooling densities. The maximum laser operation temperature decreases, confirming our new asymmetric waveguide structure improves laser thermal characteristics. The remainder of this paper is organized as follows:

In Sections 2, we introduce the device structure. We present the theoretical models and material parameters in Section3. We discuss the simulation results in Section 4.

2. LASER STRUCTURE

The simulation example in this article is a typical InGaAsP multi-quantum well (MQW) laser diode grown on InP. MQW active region consists of six 6-nm thick 1.2% compressively strained InGaAsP quantum wells. Large compressive strains are preferred in order to reduce the threshold and increase the gain coefficient. Since 10 nm thick barriers exhibit no strain; the barrier thickness of the walls is selected as 10 nm to avoid any bounded state coupling among different wells. By applying MQW structure to the active region of the laser, the performances of the laser such as threshold current, temperature characteristics, and modulation frequency were significantly improved and MQW became an essential technology for realizing high-performance lasers.

In the Ref. structure, the MQW stack is sandwiched between a pair of un-doped 170 nm-thick lattices matched InGaAsP separate confinement layer (SCLs), which act as a symmetric waveguide (conventional design). Above and below the waveguide in the structure, heavily doped p and n-type (2×10^{24} m^{-3}) InP cladding layers are used to improve electrical current injection. A highly doped p-InP contact layer is employed to complete the entire laser structure. In the New structure, an un-doped 170 nm-thick lattice matched InGaAsP interlayer between the n-SCL and n-cladding layer is introduced and the other parts of the laser structure remain unchanged. The Fabry-Perot resonator lengths are considered 500 μm. Both the lasers facets are given a reflectivity of 32%. The layer composition, doping level, and thickness for each of the layers in the New structure are given in Table 1.

Table 1. *The epitaxial asymmetric layer structure.*

Layer	Doping (m^{-3})	Thickness (μm)
n-InP (substrate)	2×10^{24}	40
InP (n- cladding)	2×10^{24}	1.3
i-$In_{0.932}Ga_{0.068}As_{0.15}P_{0.75}$ (n-interlayer)	Un-doped	0.17
i-$In_{0.87}Ga_{0.13}As_{0.28}P_{0.72}$ (n-SCL)	Un-doped	0.17
i-$In_{0.87}Ga_{0.13}As_{0.28}P_{0.72}$ (Barrie×7)	Un-doped	0.01
i-$In_{0.936}Ga_{0.064}As_{0.51}P_{0.49}$ (QW×6)	Un-doped	0.006
i-$In_{0.87}Ga_{0.13}As_{0.28}P_{0.72}$ (p-SCL)	Un-doped	0.17
InP (p- cladding)	2×10^{24}	0.02
p-InP (contact)	2×10^{24}	1.3

3. LASER MODELS AND MATERIAL PARAMETERS

A three- dimensional laser model, which combines carrier transport, optical gain computation, wave-guiding and heat- flux, is employed in Photonic Integrated Circuit Simulator in 3D (PICS3D). The electrical behavior of an InP-based semiconductor device is described with finite-element drift-diffusion model in this package. The finite-element model of carriers includes Fermi statistics and thermoionic of hetero-barriers. Gain calculations are based on 4×4 k.p band structure computations for the strained quantum wells. The software solves the scalar Helmholtz equation to obtain a transverse component of the optical field [15].

For thermal simulation, software solves the steady-state heat-flux equation:

$C_p\rho\partial T/\partial t=\nabla. k_L\nabla T+ H_{heat}$ (1)

where k_L is lattice thermal conductivity, C_p is the specific heat and ρ is the density of the material. H_{heat} is the heat source. The heat sources can be separated into Joule heat, recombination heat, Thomson heat, Peltier heat and optical absorption heat [16].

In the semiconductor lasers, carriers move from higher electrostatic potential to lower potential and the corresponding energy difference is typically absorbed by lattice as Joule heat:

$H_J = J^2_n/(q\mu_n n)+ J^2_p/(q\mu_p p)$ (2)

where J_n is electron current density and J_p is hole current density; and n and p are electron and hole densities, respectively; Joule heat is proportional to the electrical resistance of the material; μ_n is electron mobility and μ_p is hole mobility [16].

When an electron-hole pair recombines, the energy either converts to a photon or turns in to heat. For each recombined electron-hole pair, the amount of released heat is proportional to the difference between the quasi-Fermi levels:

$H_{rec} = R_{non\text{-}Radiative} (E_{Fn} – E_{Fp})$ (3)

where $R_{non\text{-}Radiative}$ is non-radiative recombination rate [14].

The Peltier heat comes from the change in the thermoelectric power when an electron-hole pair recombines. Electron-hole recombination causes cooling of carriers above the Fermi level, which fill the now empty spots at the Fermi level. This contribution is related to the thermoelectric power P_p and P_n of holes and electrons, respectively:

$H_p = q R_{tot} T (P_n– P_p)$ (4)

T qP_n and T qP_p are the average excess energies of carriers above the quasi-Fermi level and R_{tot} is total recombination rate [16].

Thomson heat is transferred between carriers and lattice as current flows along a gradient of the thermoelectric power:

$H_T = -Tq (J_n\nabla P_n + J_p\nabla P_p)$ (5)

A dramatic example is an interface between different semiconductors. When entering a material with a lower conduction band edge, electrons suddenly exhibit excess kinetic energy (hot electrons) that is eventually dissipated to the lattice. In the opposite direction, electrons need to receive extra energy from the lattice to leave the quantum well. Therefore, Thomson heat can be positive or negative (cooling) [16].

When optical waves penetrate a material, their energy can be partially or fully absorbed. The absorption heat can be simply given as:

$H_A=\alpha_0\varphi_{ph}h\nu$ (6)

where α_0 and φ_{ph} are absorption coefficient and photon flux density, respectively, and $h\nu$ is photon energy [16].

Radiative heat is a cooling source associated with the emission of a photon (photon emission requires energy and removes heat from lattice) [16]:

$H_{rad}= -G (E_{Fn} – E_{Fp})$ (7)

where G is photon generation rate.

For thermal simulation, three types of thermal boundary conditions are distinguished for the heat flux equation; i.e., Dirichlet, Neumann, and mixed conditions. The Dirichlet type simply specifies the temperature T_b at the boundary, and it is appropriate for device mounting onto a heat sink with small thermal resistance [16]:

$T_b = T_{sink}$ (8)

where T_{sink} denotes the ambient temperature. With larger external thermal resistance R^{sink}_{th}, the heat sink temperature T_{sink} becomes a function of the heat power.

In this case, the mixed boundary condition for the surface-normal heat flux applies [16]:

$$\boldsymbol{v}\boldsymbol{J}_{heat} = \frac{T_b - T_{ext}}{A_{th}R^{sink}_{th}} \quad (9)$$

with the thermal contact area A_{th} and the external temperature T_{ext} on the other side of the heat sink. This boundary condition considers an unknown but uniform boundary temperature T_b. Here, $\boldsymbol{v}$ is unit normal vector and $\boldsymbol{J}_{heat}$ is the heat flux density.

The boundary temperature becomes non-uniform with small simulated device

regions or with similar thermal conductivities on both sides of the boundary. In that case, external regions must be included in the heat flux equation. Most boundaries of a typical device exhibit negligible heat flux, which is described by the Neumann condition [16]:

$$\boldsymbol{v J_{heat} = 0} \quad (10)$$

This equation is often the default thermal boundary condition in device simulation software that we used in our simulation. In this study, we assumed that bottom contact has a lattice temperature and top contact connected to a thermal conductor with 80℃ external temperature.

The inclusion of material parameters is of paramount importance for device simulation. These parameters depend on the material composition and may be different for every layer in the device [15]. For semiconductors, these properties include band gap, effective mass (m_0), lattice constant, Luttinger parameters (γ_i), elastic constant (C_{ij}), Hydrostatic deformation potential (a_v), Shear deformation potential (b), specific heat (C_p), thermal conductivity (k_L), and refractive index (n_r). Mentioned material parameters for the compounds are computed from parameters of constituent ternary compounds using linear interpolation formulas [15]:

$$T(\mathrm{A_xB_{1-X}C_yD_{1-y}}) = [\mathrm{x}(1-\mathrm{x})[\mathrm{yT_{ABC}(x)} + (1-\mathrm{y})\mathrm{T_{ABD}(x)}] + y(1-y)[x\mathrm{T_{ACD}(y)} + (1-x)\mathrm{T_{BCD}(y)}]]/[x(1-x)+y(1-y)] \quad (11)$$

where x and y are the molar fractions and T is the ternary material parameter.

Parameters of ternary alloys AB_xC_{1-x} are usually given as [15]:

$$T(\mathrm{A_xB_{1-X}C}) = \mathrm{x}B(\mathrm{AC}) + (1-\mathrm{x})B(\mathrm{BC}) \quad (12)$$

where x is the molar fraction and B is the binary material parameter.

The composition dependence of the bandgap for $In_{1-x}Ga_xAs_yP_{1-y}$ is:

$$\mathrm{E_g}\left(\mathrm{In_{1-x}Ga_xAs_yP_{1-y}}\right) = 1.347 - 0.788\mathrm{y} + 0.149\mathrm{y}^2 - 4.1\times10^{-4}\left[\mathrm{T}^2/\left(\mathrm{T}+136\right)\right] + 8.4633030\times10^{-2} \quad (13)$$

The material parameters of the binary semiconductor used in the simulation are listed in Table 2 [17].

The carrier mobility is the key material parameter in transport simulations. We employ the Caughey-Thomas approximat-ion for the mobility as a function of carrier density [17]:

$$\mu(N) = \mu_{min} + \frac{\mu_{max}-\mu_{min}}{1+(\frac{N}{N_{ref}})^{\alpha}} \quad (14)$$

where μ_{max} is the maximum mobility (no doping) and μ_{min} is the minimum mobility for high doping densities. For all the semiconductors in this device, the temperature dependence of the mobility is given as:

$$\mu(T) = \mu(\frac{T}{300})^{\delta_0} \quad (15)$$

The mobility parameters for InP and InGaAP are shown in Table 3 and Table 4, respectively. The multi-quantum well simulation parameters are summarized in Table 5 [17].

InGaAP refractive index for different layers in the device is computed by [17]:

$$n_r = 3.167 + 0.314y \quad (16)$$

The spontaneous recombination rate is obtained from the integration of the emission spectrum in the quantum wells. For passive layers radiative recombination coefficient is assumed to be $2\times10^{-16}m^3s^{-1}$.

Table 2. *The material parameter of the binary semiconductor used in this study.*

Parameter	Unit	GaAs	InAs	InP
m_c	m_0	0.0665	0.027	0.064
γ_1	-	6.85	19.67	6.35
γ_2	-	2.1	8.37	2.08
γ_3	-	2.9	9.29	2.76
a_0	*Å*	5.65325	6.058	5.869
C_{11}	*GPa*	1181	8329	1022
C_{12}	*GPa*	532	452.6	579
a_v	*eV*	1.16	1	0.6
b	*eV*	-2.0	-1.8	-2.0
C_p	*Ws/gK*	0.327	0.352	0.311
k_L	*W/Kcm*	0.27	0.44	0.68
n_r	-	3.65	3.892	3.167

4. SIMULATION RESULTS AND DISCUSSION

It is well know that the heating effect is very important for semiconductor laser in almost all applications. The heat generated by a semiconductor laser often forces the designer to include an additional cooling system and therefore increases the cost of the application. The heating effect is more important for high power semiconductor lasers where the device temperature determines the maximum power. From the point of view of simulation and modeling the concern is two-fold. First, the temperature distribution from all possible heat sources must be detected. Identifying this distribution involves a much large simulation area than small region near the p-n junction. Thus, how to flow the heating power through the whole substrate as well as from any wire bonds must be considered. Second, the heating effects on laser performance must be considered. In other words, the accurate degradation of power and efficiency due to non- uniform temperature distribution must be evaluated. This task is not trivial at all because all variables and material parameters are temperature dependent. Both these two concepts are involved in our study [17].

Figure 1 shows the continuous-wave light output power and voltage of the Ref.

Table 3. *InP mobility parameters.*

Parameter unit	μ_{min} $m^{-2}V^{-1}S^{-1}$	μ_{max} $m^{-2}V^{-1}S^{-1}$	N_{ref} m^{-3}	α -	δ_0 -
electrons	0	0.45	1.69×10^{23}	0.436	1.25
holes	0	0.036	9.6×10^{20}	0.4	2.2

Table 4. *InGaAsP mobility parameters.*

Parameter unit	μ_{min} $m^{-2}V^{-1}S^{-1}$	μ_{max} $m^{-2}V^{-1}S^{-1}$	N_{ref} m^{-3}	α -	δ_0 -
electrons	0	0.45	1×10^{24}	0.4	1.25
holes	0	0.036	9.6×10^{20}	0.4	2.2

Table 5. *InGaAsP multi quantum well simulation parameters.*

Parameter	Unit	Value
Auger recombination constant (electron)	m^3s^{-1}	3.5×10^{-41}
Auger recombination constant (hole)	m^3s^{-1}	3.5×10^{-41}
Minority carrier lifetime (electron)	s	1×10^{-7}
Minority carrier lifetime (hole)	s	1×10^{-7}
Thermal conductivity	$WK^{-1}m^{-1}$	46
Constant background loss coefficient	m^{-1}	4000
Free carrier absorption coefficient(electron)	m^2	2×10^{-22}
Free carrier absorption coefficient(hole)	m^2	24×10^{-22}

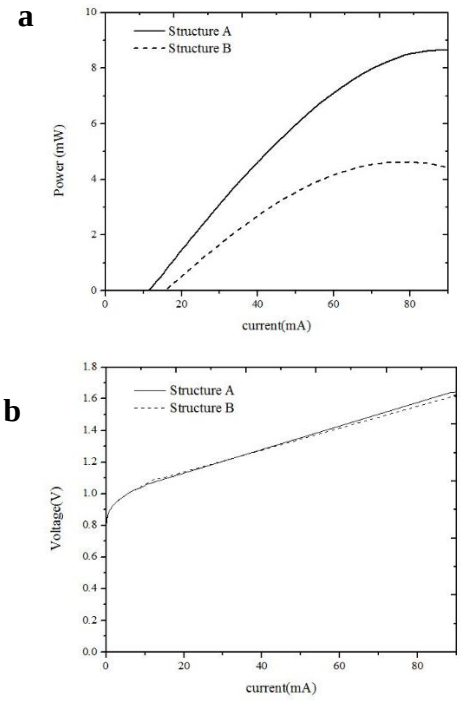

Figure 1. *(a) Continuous-wave optical light output power. (b) Voltage vs current at 80℃ stage temperature.*

Figure 1 shows the continuous-wave light output power and voltage of the Ref.

structure and the new structure against the driving current by considering thermal effects for a 80℃ stage temperature. Based on Figure 1, the output power and threshold current are improved evidently, which is attributed to the suppression of electron leakage in the New structure [18]. The slope efficiency is also improved. This result is in agreement with other publication [12, 13]. The voltage-current plot shows that the New structure voltage does not change significantly. Thus, the New structure performance is optimized because of using the asymmetric waveguide structure.

The two-dimensional temperature distributions of the Ref. structure and the New structure at an injection current of 90 mA and a stage temperature of 80℃ are shown in Figure 2 and Figure 3, respectively. As can be seen, the temperature distributions of the devices are similar to each other. As the height of devices (Y-Axis) increases, the temperature also increases. The temperature is uniform through the width of the devices (X-Axis). The p-doping layers temperature is higher than the active regions and n-doping layers temperatures. Heat is generated in semiconductor laser whenever physical processes transfer energy to the device lattice. The flow of carriers through a semiconductor laser layer is accompanied by frequent carrier scattering by phonons, leading to continuing energy loss to the laser structure that lead to the temperature of active region being much greater than the heat sink. By comparing Figure 2 and Figure 3, it can be seen that the maximum temperature of the New structure is reduced by 10℃.Therefore, it can be claimed that our new proposed asymmetric waveguide structure improves the semiconductor laser thermal stability.

The electrical resistances of interfaces and highly p-doping layers, as well as non-radiative recombination in the active layers, are main heat sources in semiconductor lasers [19]. The vertical Joule heat power density profiles of the two devices are illustrated in Figure 4. It has been found that the Joule heating is confined to a region of a few microns near the p- doping layer interfaces, since the low mobility holes and high electric field exist very close to these interfaces.

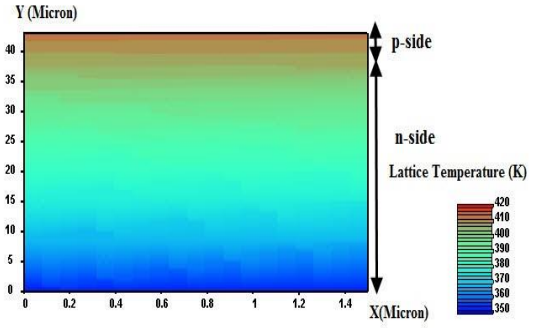

Figure 2. *Temperature distribution of Ref. structure at an injection current of 90 mA and a stage temperature of 80℃.*

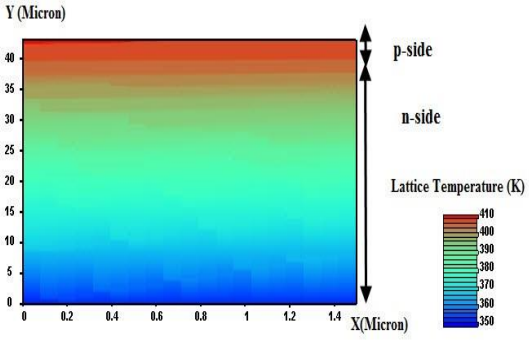

Figure 3. *Temperature distribution of New structure at an injection current of 90 mA and a stage temperature of 80℃.*

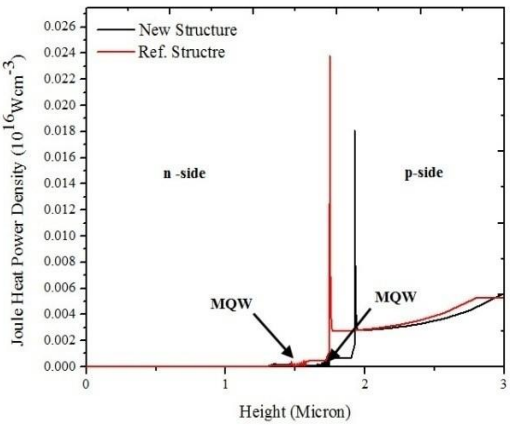

Figure 4. *Vertical Joule heat power*

density at an injection current of 90 mA and a stage temperature of 80℃.

The asymmetric waveguide structure dec- reases Joule heating in the semiconductor laser structure.

In Figure 5, vertical electric field versus height is plotted. It is found that the peak of the electric field is located near the doped regions and decreases using the asymmetric waveguide structure. It is known that the current density of electrons and hole is proportional to the magnitude of the electric field. According to Eq.2, the Joule heating varies by the changes of carrier current densities [15]. Thus, the electric field reduction causes decrease the electron and the hole current densities and as a consequence, the Joule heating decreases in New structure.

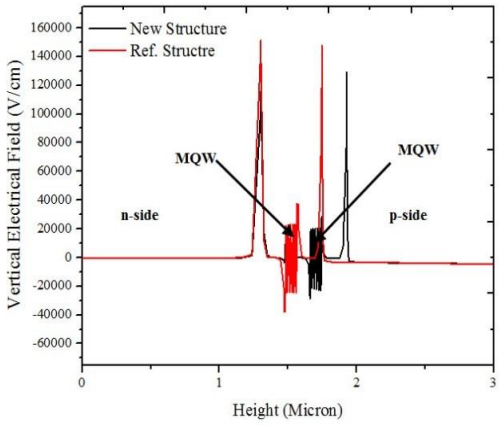

Figure 5. *Vertical electrical field at an injection current of 90 mA and a stage temperature of 80℃.*

The recombination heat source around the active region accounts for the energy of the order of the bandgap dissipated to the lattice by non-radiative recombination (Eq. 3). Each recombining electron-hole pair releases its energy, which is immediately transferred to the lattice unless it is transferred to the radiation field [20]. As depicted in Figure 6, recombination heat power density increases in New structure laser; because of the reduction of the leakage current, the presence of carriers in the active region increases, which leads to an increase in the non-radiative recombination and its generated heat.

Figure 7 compares radiation heat power density in two structures. Radiative heat is a cooling source associated with the emission of a photons. Since carrier density increases in the New asymmetric structure active region, stimulated recombination rate and photon density increase in the quantum wells and as a consequence the radiation cooling increases in the asymmetric waveguide laser. In other words, the numbers of photons that can leave the quantum wells and enhance the optical wave increases. Optical wave amplification is the main reason for increasing the output power in New structure.

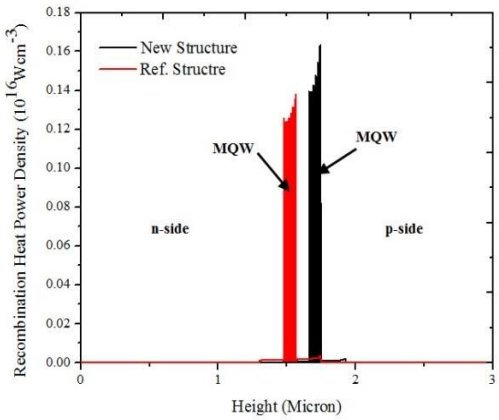

Figure 6. *Vertical Recombination heat power density at an injection current of 90 mA and a stage temperature of 80℃.*

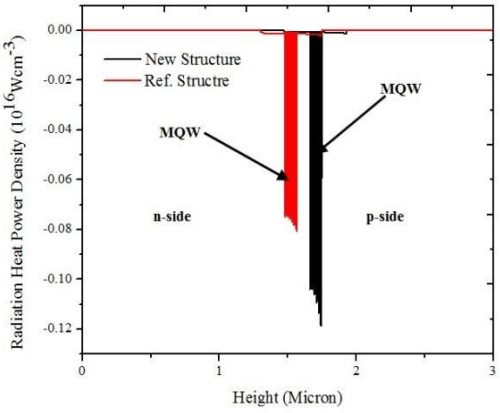

Figure 7. *Vertical Radiation heat power density at an injection current of 90 mA and a stage temperature of 80℃.*

Next heating source that was studied is Peltier heat. Figure 8 shows Peltier heat density in different laser structures. Since electrons and holes have separate quasi-Fermi energies, one can define Peltier heat exchange terms for each type of carrier at the heterointerfaces and then add them together to yield the total bipolar thermoelectric heat source distribution (Eq. 4). As the carriers enter the waveguide region, their average transport energy is reduced, causing heat to be generated at the cladding/SCL interfaces. A portion of the injected carriers leaks out of the waveguide region without recombining and leads to thermoelectric cooling at the heterointerfaces. A similar argument can be used to estimate thermoelectric cooling or heating at the QW interfaces [21]. Figure 8 confirms that the asymmetric waveguide does not change Peltier heating significantly.

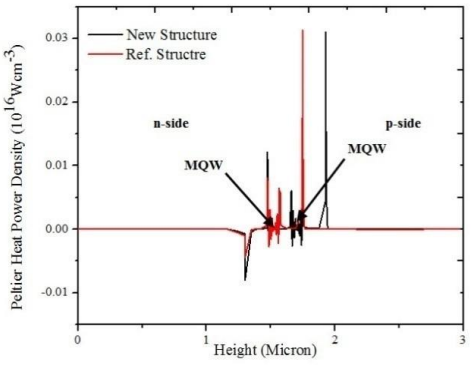

Figure 8. *Vertical Peltier heat power density at an injection current of 90 mA and a stage temperature of 80 ℃.*

Thomson heat power density of two structures is plotted in Figure 9. Electrons need to receive extra energy from the lattice to leave the quantum well. Therefore, Thomson heat is negative (cooling) in the quantum wells. Increasing the electron density in the quantum wells leads to an increase in electron current density, and thus a consequent rise in New structure Thomson heat (Eq. 5).

Figure 10 shows absorption heat in two structures. By comparing Figure 10 with Figures 4, 6, and 8, we notice that absorption heat is smaller than other heating sources. Absorption heat increases in asymmetric structure due to the increased photon density (Eq. 6).Figures 7 and 10 confirm that in New structure photons are more effective in creating an optical field instead of being absorbed by semiconductor laser layers.

5. CONCLUSION

In this work, asymmetric waveguide structure was employed to replace the conventional symmetric waveguide. The performance characteristics of InGaAsP laser diodes with the symmetric and asym-

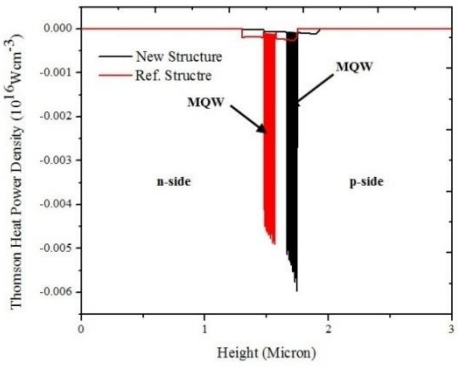

Figure 9. *Vertical Thomson heat power density at an injection current of 90 mA and a stage temperature of 80 ℃.*

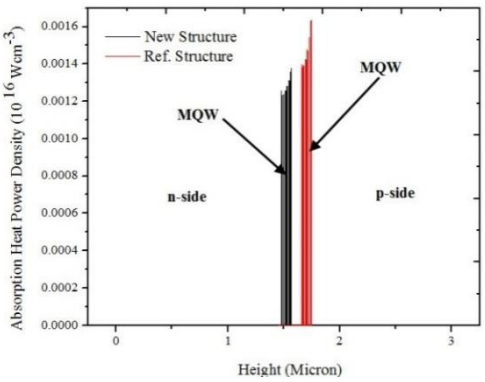

Figure 10. *Vertical Absorption heat power density at an injection current of 90 mA and a stage temperature of 80 ℃.*

metric structures are numerically investigated by using the simulation software PICS3D. The results indicate that asymmetric waveguide leads to semiconductor laser shows higher output light power and slope efficiency. Joule heating decreases and recombination heat

increases, but heat dissipation occurs more effectively due to increased cooling densities. We found that the maximum laser operation temperature decreases, confirming that our new asymmetric waveguide structure improves laser thermal characteristics.

ACKNOWLEDGEMENT

We express our sincere appreciation to the Managers of Cross Light Inc. for providing us with the advanced three-dimensional PICS3D simulation program (version 2008.12) and their kind support.

REFERENCES

1. Bahrami Yekta, V., Kaatuzian, H., (2014). "Simulation and Temperature Characteristics Improvement of 1.3 μm AlGaInAs Multiple Quantum Well Laser", *International Journal of Optics and Applications*, 4: 46-53.
2. Jabbari, M., Moravvej-Farshi, M. K., Ghayour, R., Zarifkar, A., (2011). "The Effects of Strained Multiple Quantum Well on the Chirped DFB-SOA All Optical Flip-Flop", *Int. J. Nanosci. Nanotechnol*, 7: 190-196.
3. Gonul, B., Cak, F. Ko., Toktam, H., Oduncuoglu,M., (2004). "Theoretical Comparison of the Band Alignment of Conventionally Strained and Strain-Compensated Phosphorus- Aluminum- and Nitrogen-Based 1.3 μm QW Lasers", *Chinese Journal of Physics*, 42: 764-775.
4. Rajaei, E., Borji, M. A., (2016). "Energy Levels of InGaAs/GaAs Quantum Dot Lasers with Different Sizes", *Int. J. Nanosci. Nanotechnol*, 12: 45-53.
5. Piprek, J., Abraham,P., Bowers, J. E., (2000). "Self-consistent analysis of high-temperature effects on strained layer multi quantum-well In-GaAsP-InP lasers", IEEE *J. Quantum Electron*, 36: 366-374.
6. Tsai, C. Y., Eastman, L. F., Lo, Y. H., (1993). "Hot carrier and hot phonon effects on high-speed quantum well lasers", *Appl. Phys. Lett*., 63: 3408–3410.
7. Ng, W. C., Liu, Y., Hess, K., (2004). "Lattice Temperature Model and Temperature Effects in Oxide-Confined VCSEL's", *Journal of Computational Electronics*, 3: 103-116.
8. Piprek, J., White, J. K., Spring Thorpe, A. J., (2000). "What limits the maximum output power of long wavelength AlGaInAs–InP laser diodes?", *IEEE J. Quantum Electron*, 38 : 1253–1259.
9. Liu, Y., Ng, W. C., Choquette, K.D., Hess, K., (2005). "Numerical investigation of self-heating effects of oxide confined vertical-cavity surface-emitting lasers", *IEEE J. Quant. Electron*, 41: 15-25.
10. Etienne, B., Shah, J., Leheny, R. F., Nahory, R. E., (1982). "Influence of hot carriers on the temperature dependence of threshold in 1.3-μmInGaAsP lasers", *Appl. Phys. Lett*., 41: 1018–1020.
11. Slipchenko, S. O., Vinokurov, D. A., Pikhtin, N. A., Sokolova, Z. N., Stankevich, A. L., Tarasov,I. S., Alferov, Z. I., (2004). "Ultralow internal optical loss in separate-confinement quantum well heterostructures", *Semiconductor*, 38: 1430-1439.
12. Tijero, J. M. G., Odriozola, H., Borruel, L., Esquivias, I., Sujecki, S., Larkins, E. C., (2007). "Enhanced Brightness of Tapered Laser Diodes Based on an Asymmetric Epitaxial Design", *IEEE. Photon. Tech. Lett*, 19:1640-1642.
13. Bour, D. P., Kneissl, M., Van de Walle, C. G., Evans, G. A., Romano, L. T., Northrup, J., Teepe, M., Wood, R., Schmidt, T., Schoffberger, S., Johnson, N. M., (2000). "Design and performance of Asymmetric Waveguide Nitride Laser Diodes", *IEEE J. Quant. Electron*, 36: 184-191.
14. Available online at WWW.Crosslight.Com.
15. Danesh kaftroudy, Z., Rajaei, E., (2011). "Thermal simulation of InP- based 1.3 μm vertical cavity surface emitting laser with AsSb- based DBRs", *Optics Communications*, 284: 330-340.
16. Piprek, J., (2003). "*Semiconductor optoelectronic devices*", Elsevier Science, San Diego.
17. PICS3D User's manual version 2008.12.
18. Li, X., Zhao, D. G., Jiang, D. S., Chen, P., Liu, Z. S., Zhu, J. J., Shi, M., Zhao, D. M., Liu, W., (2016). "Suppression of electron leakage in 808 nm laser diodes with asymmetric waveguide layer", *J. Semicond.*, 37: 014007-1-014007-4.
19. Li, X., (2009). "*Optoelectronic Devices: Design, Modeling and simulation*", Cambridge University Press.
20. Piprek, J., (2005). "*Optoelectronic Devices: Advanced Simulation and Analysis*", Springer.
21. Pipe, K. P., Ram, R. J., Shakouri, A., (2002). "Internal Cooling in Semiconductor Laser Diode", *IEEE. Photon. Tech. Lett.*, 14: 453-455.